Creation of disease-inspired biomaterial environments to mimic pathological events in early calcific aortic valve disease

Ana M. Porras[a], Jennifer A. Westlund[a], Austin D. Evans[a], and Kristyn S. Masters[a,b,1]

[a]Department of Biomedical Engineering, University of Wisconsin–Madison, Madison, WI 53705; and [b]Department of Medicine, University of Wisconsin–Madison, Madison, WI 53705

Edited by David J. Mooney, Harvard University, Cambridge, MA, and accepted by Editorial Board Member Rakesh K. Jain December 8, 2017 (received for review March 20, 2017)

An insufficient understanding of calcific aortic valve disease (CAVD) pathogenesis remains a major obstacle in developing treatment strategies for this disease. The aim of the present study was to create engineered environments that mimic the earliest known features of CAVD and apply this in vitro platform to decipher relationships relevant to early valve lesion pathobiology. Glycosaminoglycan (GAG) enrichment is a dominant hallmark of early CAVD, but culture of valvular interstitial cells (VICs) in biomaterial environments containing pathological amounts of hyaluronic acid (HA) or chondroitin sulfate (CS) did not directly increase indicators of disease progression such as VIC activation or inflammatory cytokine production. However, HA-enriched matrices increased production of vascular endothelial growth factor (VEGF), while matrices displaying pathological levels of CS were effective at retaining lipoproteins, whose deposition is also found in early CAVD. Retained oxidized low-density lipoprotein (oxLDL), in turn, stimulated myofibroblastic VIC differentiation and secretion of numerous inflammatory cytokines. OxLDL also increased VIC deposition of GAGs, thereby creating a positive feedback loop to further enrich GAG content and promote disease progression. Using this disease-inspired in vitro platform, we were able to model a complex, multistep pathological sequence, with our findings suggesting distinct roles for individual GAGs in outcomes related to valve lesion progression, as well as key differences in cell–lipoprotein interactions compared with atherosclerosis. We propose a pathogenesis cascade that may be relevant to understanding early CAVD and envision the extension of such models to investigate other tissue pathologies or test pharmacological treatments.

calcific aortic valve disease | glycosaminoglycans | inflammation | oxidized LDL

Calcific aortic valve disease (CAVD) is a prevalent aortic valve disorder (1) for which there is no treatment other than total valve replacement. Many investigations have focused on characterizing the features of end-point stenosis (2–4), but even early stages of CAVD are associated with an increase in cardiovascular (5) and all-cause mortality (6). Moreover, CAVD is hypothesized to reach a "point of no return," beyond which pharmaceutical intervention is unlikely to stop or slow its progression (7). However, while histological analyses of native valves can provide snapshots of disease features, they cannot tell us the order in which these pathological events occur. Our limited knowledge of the sequence of events in CAVD pathogenesis provides a significant obstacle in developing treatments for this disease.

Analyses of sclerotic lesions have identified three features that emerge early in the disease process: (*i*) reorganization of the extracellular matrix (ECM), (*ii*) lipoprotein deposition and oxidation, and (*iii*) infiltration of immune cells (8–14). These events appear to precede other hallmarks, such as myofibroblastic or osteoblastic differentiation of valvular interstitial cells (VICs) and elevated VIC proliferation, apoptosis, angiogenesis, and calcification. In this work, we aim to generate a platform that enables us to determine the relationship between the three aforementioned features that are found in early CAVD and to decipher their sequence in an in vitro context.

The ECM reorganization in early CAVD occurs in the form of proteoglycan (PG) and glycosaminoglycan (GAG) enrichment (12). Specifically, valve leaflets become significantly thickened due to increased amounts of hyaluronic acid (HA)- and chondroitin sulfate (CS)-containing PGs throughout the leaflet (13, 15). Oxidized low-density lipoprotein (oxLDL) is also prevalent in these GAG-enriched valves (12). Examination of mildly sclerotic valves from pigs with familial hypercholesterolemia suggests that both GAG enrichment and the deposition of oxLDL occur before macrophage infiltration (11).

GAGs such as HA have been recognized as important elements of healthy valve function, as HA depletion is sufficient to induce pathological outcomes (16). HA has been the only GAG used in the construction of valve scaffolds, and VICs thrive in biomaterial scaffolds containing HA (17, 18). However, previous work with these materials has not focused on the role of HA in early disease progression, nor has it tailored the HA content to match that found in native valves. Most previous HA-containing materials have also lacked the presence of collagen, which is the most prevalent ECM component in the valve and essential for maintaining a healthy VIC phenotype (19). Additionally, all prior studies have used VICs that express a myofibroblastic or osteoblastic phenotype, which is not consistent with the phenotype of VICs during early stages of CAVD (2, 20, 21); methods

Significance

Due to an insufficient understanding of the mechanisms that drive its progression, there is currently no treatment for calcific aortic valve disease (CAVD) other than valve replacement. In this report, we describe the generation of engineered environments that mimic features found in early CAVD. By combining these engineered models of valve disease with other exogenous cues present during CAVD, we were able to propose a previously unidentified cascade of pathological events and identify specific extracellular components that are critical in regulating this process. These findings demonstrate the utility of engineered in vitro models to perform systematic, controlled studies of events related to disease progression that may lead to future identification of potential targets for therapeutic interventions.

Author contributions: A.M.P. and K.S.M. designed research; A.M.P., J.A.W., and A.D.E. performed research; A.M.P., J.A.W., A.D.E., and K.S.M. analyzed data; and A.M.P. and K.S.M. wrote the paper.

The authors declare no conflict of interest.

This article is a PNAS Direct Submission. D.J.M. is a guest editor invited by the Editorial Board.

[1]To whom correspondence should be addressed. Email: kmasters@wisc.edu.

This article contains supporting information online at www.pnas.org/lookup/suppl/doi:10.1073/pnas.1704637115/-/DCSupplemental.

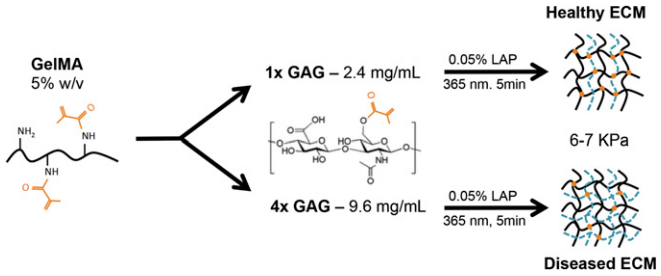

Fig. 1. Fabrication of GelMA/GAG hydrogels. Shown is a schematic of the cross-linking reaction between GelMA and GAG to yield substrates with a healthy (1×, 2.4 mg/mL) or pathological (4×, 9.6 mg/mL) amount of GAG. GelMA with varying degrees of methacrylate functionalization was employed to maintain constant material stiffness upon incorporation of increased GAG.

to generate VICs that express a native, quiescent phenotype have only recently been described (22, 23).

Thus, in this work, we describe the generation of an in vitro platform intended to mimic several characteristics of valvular lesions in early CAVD, with a focus on investigating the role of ECM composition in stimulating behaviors related to disease progression. To represent the GAG enrichment that is found in early lesions, a hybrid biomaterial consisting of both methacrylated gelatin and methacrylated HA or CS was constructed to provide varied levels of GAG content with a constant collagen-based background. These two GAGs are the most prevalent in native valves, and they were studied independently of each other because their structural and biological differences suggest they likely play differential roles in CAVD progression. To approximate the VIC phenotype found in native valves, VICs exhibiting a quiescent phenotype (qVICs) (21, 23) were seeded on these materials. These culture platforms were then combined with LDL or oxLDL to decipher the relationships between GAG enrichment, LDL/oxLDL deposition, and inflammatory activity. Our findings from this disease-inspired in vitro model revealed pathological relationships in the context of valvular disease which we hope will ultimately advance our understanding of in vivo CAVD pathogenesis.

Results

Synthesis of Methacrylated Gelatin/GAG Hydrogel Substrates. Hydrogel culture substrates consisting of copolymerized networks of methacrylated gelatin (GelMA) and methacrylated GAGs were synthesized to mimic the extracellular environment present in aortic valve leaflets. Specifically, 5% wt/vol GelMA was mixed with methacrylated HA or CS at either 2.4 mg/mL or 9.6 mg/mL to mimic the collagen: HA ratio present in healthy tissues (19) and the GAG enrichment observed in diseased valves, respectively (Fig. 1 and Fig. S1) (11). These two GAG concentrations are referred to as "1×" and "4×" throughout the figures and text, and the focus of subsequent experiments was to understand the consequences of GAG enrichment on events related to lesion progression, rather than elucidate the factors that caused the initial ECM dysregulation. Although the GelMA concentration remained constant for all formulations, GelMA batches with different degrees of functionalization were mixed to maintain the Young's modulus at 7 ± 1 kPa.

GAG Enrichment Attenuates the Production of Inflammatory Factors. Previous work identified the infiltration of immune cells as an early feature of CAVD that follows GAG enrichment (11). Thus, we first applied our biomaterial platform to determine whether GAG enrichment is sufficient to directly enhance the inflammatory activity of VICs. Specifically, the production of inflammatory cytokines by VICs was measured following VIC culture on hydrogel substrates containing 1× ("healthy") or 4× ("diseased") HA or CS. In general, the presence of HA or CS was associated with decreased secretion of inflammatory cytokines (Fig. 2 *A*–*D*). For example, relative to the GelMA control, VIC secretion of IL-6 (Fig. 2*A*) remained unchanged upon incorporation of HA or CS amounts found in healthy valves, but was significantly reduced by pathological enrichment of CS. VIC production of interleukin-8 (IL-8) was reduced in the presence of either GAG and was reduced even further in environments containing pathological levels of HA or CS (Fig. 2*B*). Meanwhile, monocyte chemoattractant protein-1 (MCP-1) secretion was similar across all biomaterial conditions, with the exception of significant attenuation on 1× CS substrates relative to GelMA alone (Fig. 2*C*). Finally, the production of platelet-derived growth factor (PDGF) by VICs was significantly decreased in the presence of HA or CS compared with the GelMA control (Fig. 2*D*).

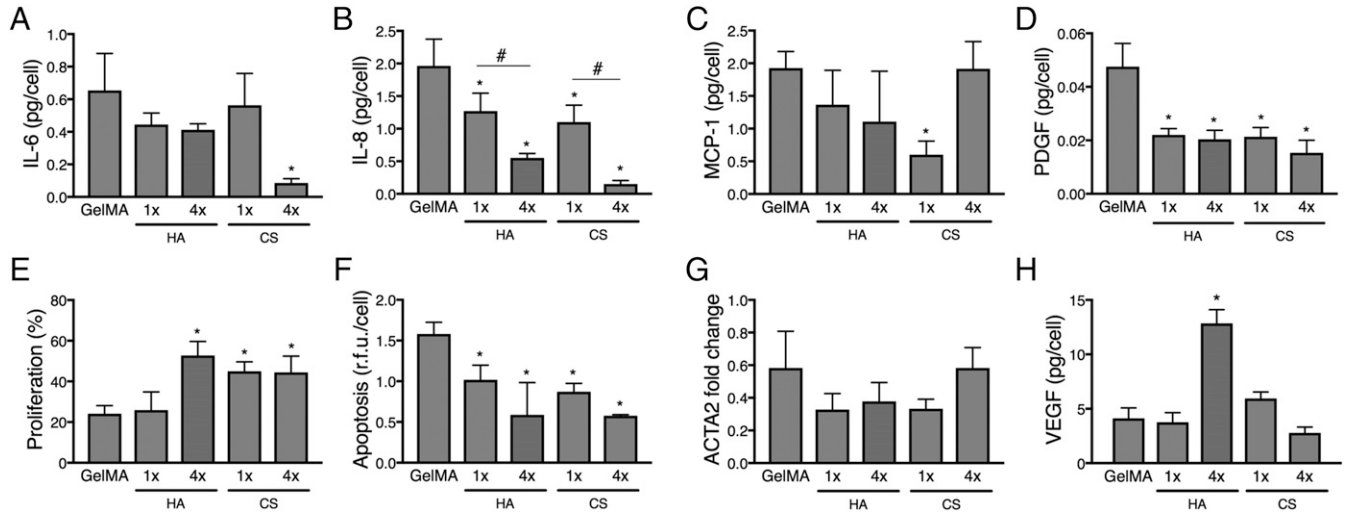

Fig. 2. Impact of GAG enrichment on inflammatory and angiogenic cytokine production and VIC activation. VICs were cultured on GelMA substrates containing HA or CS at healthy (1×) or pathological (4×) concentrations and assayed for the production of (*A*) IL-6, (*B*) IL-8, (*C*) MCP-1, and (*D*) PDGF, as well as (*E*) the percentage of proliferating cells, (*F*) apoptosis, (*G*) *ACTA2* expression, and (*H*) VEGF production. *$P < 0.05$ compared with GelMA control. #$P < 0.05$ for comparisons shown. $n = 4$.

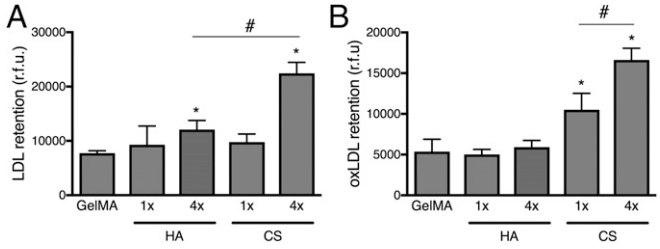

Fig. 3. Lipoprotein deposition on GelMA/GAG substrates. (*A* and *B*) Deposition of (*A*) LDL and (*B*) oxLDL on GelMA substrates containing HA or CS at healthy (1×) or pathological (4×) concentrations. *$P < 0.05$ compared with GelMA. #$P < 0.05$ for comparison shown. $n = 6$.

These findings indicated that neither HA nor CS enrichment was able to initiate increased inflammatory activity by VICs; in fact, increased levels of these GAGs appeared to suppress the secretion of inflammatory cytokines. Therefore, we next investigated the relationship between GAG enrichment and myofibroblastic activation of VICs, a different pathological event that emerges after initial ECM rearrangement and is thought to be a prominent driver in CAVD pathogenesis (2, 3, 21). Characteristics indicative of VIC activation are increased proliferation and apoptosis, as well as expression of α-smooth muscle actin (αSMA) (21). The presence of either a healthy (1×) or a pathological (4×) amount of CS was sufficient to increase cell proliferation compared with GelMA substrates containing no CS (Fig. 2*E*). Meanwhile, proliferation was unchanged relative to the GelMA control upon incorporation of 1× HA, but became elevated upon enrichment of HA to a pathological concentration (4×). In contrast, a decrease in cellular apoptosis was observed upon addition of either GAG relative to the GelMA control (Fig. 2*F*). Although an increase in proliferation can suggest VIC activation, no changes in the gene expression levels of αSMA were observed (Fig. 2*G*), where αSMA is considered the defining feature of VIC activation. Thus, GAG enrichment did not appear to directly induce either inflammatory activity or myofibroblastic differentiation. Finally, we investigated the relationship between GAG enrichment and VIC production of a proangiogenic molecule, vascular endothelial growth factor (VEGF), since angiogenesis also occurs as a later hallmark of valvular disease. VEGF production was dramatically increased by HA enrichment, but remained similar to the GelMA control in all other conditions (Fig. 2*H*). To confirm that the quiescent VICs used in this study had not experienced phenotypic drift, a subset of these analyses was repeated using naive VICs that had never been subcultured. For all markers examined (proliferation, IL-6, IL-8, and PDGF), the response of the naive VICs was similar to that obtained using quiescent VICs (Fig. S2).

GAG Enrichment Regulates the Availability of LDL and oxLDL. We next sought to determine the purpose of GAG enrichment in CAVD progression by examining whether this feature plays an indirect role in stimulating inflammation and VIC activation by regulating the availability of lipoproteins. As noted earlier, the earliest pathological features observed in CAVD have been GAG enrichment and deposition of oxidized lipoproteins (12). GAG-containing hydrogels were treated with fluorescently labeled LDL or oxLDL and assayed for lipoprotein retention. Substrates enriched in HA or CS retained significantly more LDL compared with the GelMA control, with 4× CS hydrogels exhibiting higher levels of LDL deposition than 4× HA hydrogels (Fig. 3*A*). Meanwhile, oxLDL bound preferentially to CS-containing gels compared with GelMA- and HA-containing substrates. Once again, the highest levels of oxLDL retention were achieved in environments containing a pathological amount of CS (Fig. 3*B*).

While Fig. 3 demonstrates that GAG enrichment can modulate lipoprotein retention, it was not known whether LDL or oxLDL could be responsible for stimulating downstream disease hallmarks such as inflammatory activity or activation of quiescent VICs. Thus, VICs were seeded on GelMA hydrogels and treated with LDL or oxLDL at a concentration of 25 μg/mL for 48 h (Fig. 4) to determine the response of VICs to LDL and oxLDL, independent of changes in lipoprotein availability that can occur due to differential retention by GAGs. LDL treatment had no effect on the production of inflammatory cytokines (Fig. 4 *A–D*) or VIC phenotype (Fig. 4 *E–G*), and VICs in these culture conditions did not exhibit the capacity to oxidize LDL themselves (Fig. S3). In contrast, oxLDL had a potent proinflammatory effect on VICs, as significantly higher levels of IL-6, IL-8, MCP-1, and PDGF were detected following oxLDL treatment of VICs (Fig. 4 *A–D*). Likewise, oxLDL treatment led to an increase in VIC αSMA gene expression (Fig. 4*E*), proliferation (Fig. 4*F*), apoptosis (Fig. 4*G*) compared with the untreated control, indicating that oxLDL stimulated myofibroblastic differentiation of VICs. However, neither LDL nor oxLDL was found to stimulate osteogenic differentiation of the quiescent VICs, as indicated by ALP and BMP2 gene expression (Fig. S4). Production of VEGF did not change upon treatment with either LDL or oxLDL (Fig. 4*H*). A subset of these

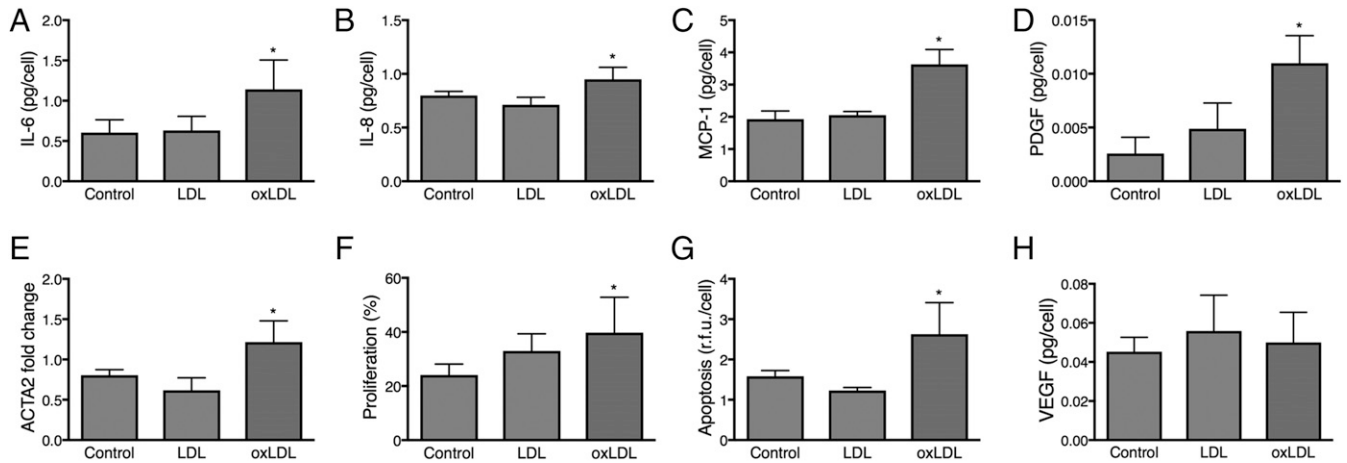

Fig. 4. Impact of LDL/oxLDL on the production of cytokines, growth factors, and VIC activation. VICs cultured on GelMA substrates and treated with 25 μg/mL LDL or oxLDL for 48 h were assayed for production of (*A*) IL-6, (*B*) IL-8, (*C*) MCP-1, and (*D*) PDGF, as well as (*E*) *ACTA2* gene expression, (*F*) proliferation, (*G*) apoptosis, and (*H*) VEGF production. *$P < 0.05$ compared with untreated control. $n = 4$.

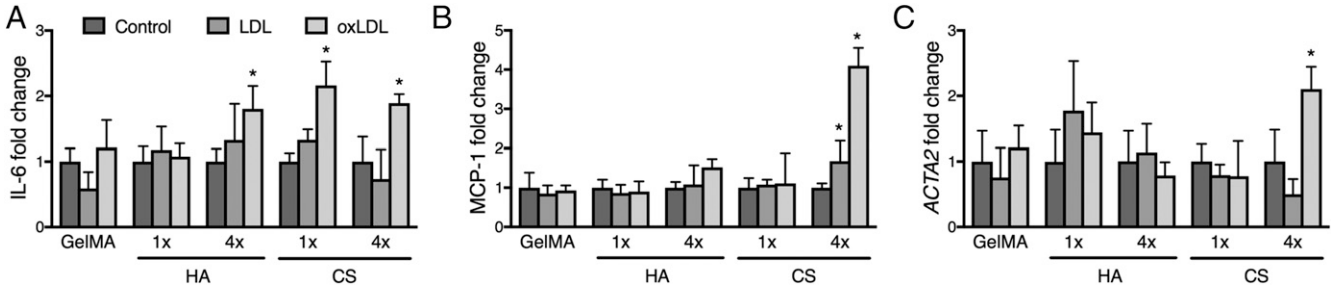

Fig. 5. VIC function in response to GAG-bound lipoproteins. VICs were cultured on GelMA/GAG hydrogels that had been pretreated with 200 μg/mL of LDL or oxLDL and rinsed to remove unbound lipoproteins. After 48 h, cultures were assessed for production of inflammatory cytokines (*A*) IL-6 and (*B*) MCP-1 as well as (*C*) myofibroblast marker *ACTA2*. **P* < 0.05 compared with the untreated control for each substrate formulation. *n* = 4.

analyses was repeated using naive VICs and found to yield similar results (Fig. S2).

Effect of Combined GAG Enrichment and Lipoprotein Exposure. The differential lipoprotein retention caused by GAG enrichment, combined with the potency of oxLDL in stimulating inflammatory cytokine secretion and VIC activation, gave rise to the hypothesis that pathological levels of GAGs act to entrap LDL/oxLDL, and the deposited oxLDL is then available to stimulate VIC dysfunction. To test this hypothesis, VICs were cultured on GelMA/GAG substrates that had been preincubated with 200 μg/mL LDL or oxLDL for 24 h, a concentration determined to yield retained oxLDL in a range relevant to earlier experiments (Fig. S5). This setup was intended to better approximate the native environment, where VICs would interact with lipoproteins that have been differentially retained by the matrix, rather than direct exposure to circulating LDL and oxLDL. VICs were cultured on GelMA/GAG substrates containing bound LDL or oxLDL for 48 h and analyzed for a subset of disease markers indicative of inflammatory activity or VIC activation. As shown in Fig. 5, pathological CS enrichment supported the retention of sufficient oxLDL to significantly increase VIC secretion of IL-6 (Fig. 5*A*) and MCP-1 (Fig. 5*B*) and expression of *ACTA2* (Fig. 5*C*) compared with culture on 4× CS alone. A combination of CS enrichment and LDL deposition also yielded significantly increased MCP-1 production by VICs, although this was the only condition where deposited LDL was able to effect changes in VIC behavior.

GAG Enrichment and oxLDL Deposition Participate in a Positive Feedback Loop. Finally, we examined whether deposited lipoproteins could regulate GAG production by VICs, thereby creating a positive feedback loop. Treatment with LDL did not significantly increase GAG synthesis by VICs, as measured by expression of CS synthase-1 (*CHSY1*, Fig. 6*A*), expression of HA synthase-3 (*HAS3*, Fig. 6*B*), secretion of sulfated GAGs (Fig. 6*C*), or secretion of HA (Fig. 6*D*). However, oxLDL did significantly increase VIC expression of *CHSY1* and *HAS3*, as well as HA deposition compared with the untreated control. The deposition of total sulfated GAGs was not affected by oxLDL, although this assay is not specific to CS alone.

VIC Production of Inflammatory Cytokines Precedes Macrophage Invasion in Vivo. To validate that the production of inflammatory cytokines observed by VICs in these in vitro experiments was relevant to the in vivo condition, leaflets from 1-y-old wild-type (1yo WT) or Rapacz hypercholesterolemic (1yo RFH) swine were examined for the presence of IL-6, PDGF-BB, and macrophages. As discussed in our previous work (11), leaflets from 1yo swine with familial hypercholesterolemia exhibit several hallmarks of early CAVD, such as abundant GAG enrichment, pathological leaflet thickening, and deposition of oxLDL; these leaflets ultimately progress to mild sclerosis. Staining for IL-6 in WT and RFH leaflets demonstrated minimal presence of this cytokine in WT animals, but a fourfold elevation in mildly diseased (RFH) leaflets (Fig. 7*A*). Meanwhile, PDGF-BB was strongly present in leaflets from WT animals, but still elevated by twofold in diseased leaflets (Fig. 7*B*). The absence of macrophages in 1yo animals (Fig. S6*A*) and cytokine presence throughout the leaflet width strongly suggest that VICs were responsible for the significant increases in IL-6 and PDGF present at this early disease stage. Macrophages were successfully detected in older (3yo) RFH animals with valvular sclerosis (Fig. S6*B*) (11).

Discussion

Disarray of the highly organized ECM normally found in the aortic valve is an important hallmark of CAVD (9, 10); specifically, GAG enrichment has been identified as a key feature during the early stages of the disease (11–13). Similarly, lipoprotein metabolism and inflammation have also been hypothesized to play a role in the progression of aortic valve sclerosis (3, 24–27). However, the limitations of existing in vivo and in vitro models have restricted our understanding of the order in which these events occur. The present study sought to understand pathological events that occur soon after early lesion development by engineering cell culture environments that mimic the ECM and other factors found in early CAVD. The results reported here suggest a sequence of events that highlights the separate contributions of individual ECM features to VIC pathobiology (Fig. 8) and reveals interactions that potentially

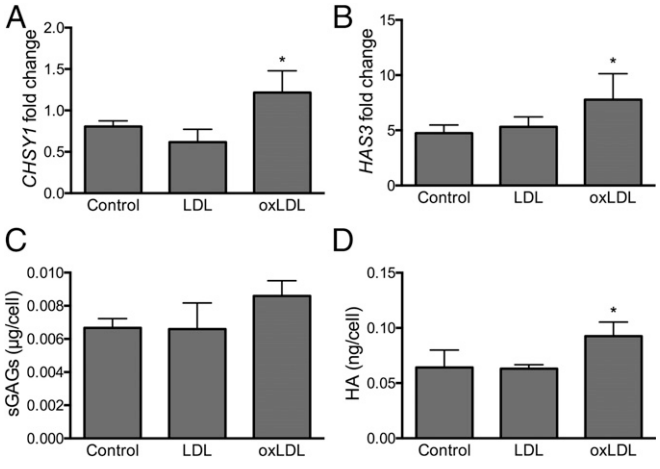

Fig. 6. Impact of LDL/oxLDL on GAG production. VICs cultured on GelMA substrates and treated with 25 μg/mL LDL or oxLDL for 48 h were assayed for expression of two enzymes responsible for synthesizing CS and HA, (*A*) CHSY1 and (*B*) HAS3, as well as the production of (*C*) sulfated GAGs and (*D*) HA. **P* < 0.05 compared with untreated control. *n* = 4.

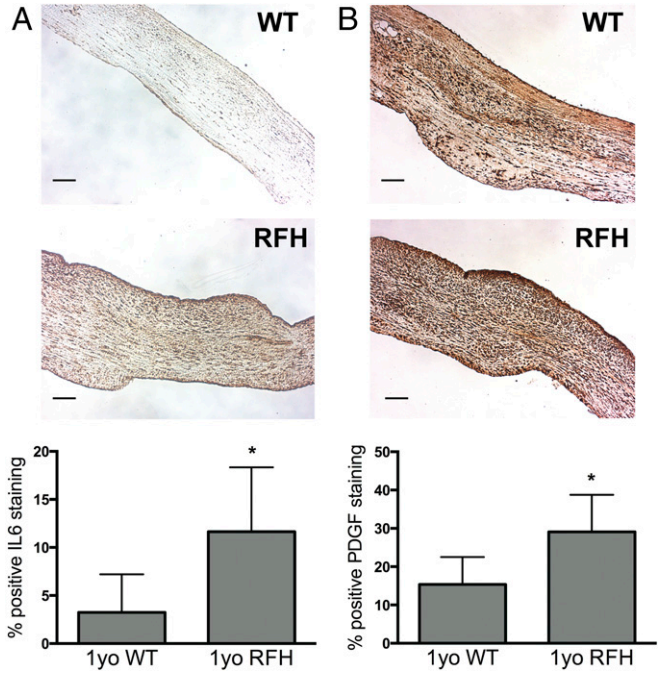

Fig. 7. Detection of inflammatory cytokines in diseased leaflets. (*A*) IL-6 and (*B*) PDGF-BB were detected in leaflets from 1yo WT swine or 1yo RFH swine, where the latter exhibit hallmarks of early CAVD. Both cytokines were significantly elevated in the diseased leaflets. *$P < 0.05$ compared with 1yo WT. $n = 3$ animals per condition, $n = 3$ samples per animal.

differentiate valve lesion progression from that of atherosclerosis. Pathological levels of HA directly stimulated VIC production of a proangiogenic factor, while pathological levels of CS were able to trap both LDL and oxLDL. In contrast to smooth muscle cell behavior in atherosclerotic lesions, VICs were generally unresponsive to LDL; however, oxLDL was a potent stimulant for the secretion of inflammatory cytokines and expression of a myofibroblastic phenotype by VICs. Examination of mildly diseased leaflets from swine with familial hypercholesterolemia confirmed VICs as the primary source of inflammatory cytokines during early-stage CAVD. Finally, oxLDL treatment induced an increase in both HA and CS production to form a positive feedback loop that may enable further lesion progression. Although the role of this cascade in the progression to later-stage events or the development of clinical CAVD has yet to be determined, use of this disease-inspired platform yielded insight into VIC behaviors that may hopefully advance us toward unraveling CAVD pathogenesis.

The ability of GAGs to regulate inflammation has been described for many other tissues (28–31). However, little is known regarding the relationship between inflammatory activity and GAGs in the context of the aortic valve. In the present study, we found that enrichment of either CS or HA to mimic early valve pathology was insufficient to induce an increase in the production of inflammatory cytokines. In fact, our findings suggest an antiinflammatory role for these GAGs in both healthy and early-disease environments. GAG enrichment was also insufficient to induce myofibroblastic differentiation of VICs; this finding is consistent with previous studies of VICs cultured in HA-rich environments, where VIC encapsulation in HA hydrogels or treatment with exogenous HA led to reduced expression of myofibroblastic markers (16, 18, 32, 33). However, one notable effect of HA enrichment in our study was a dramatic increase in VEGF production by VICs. This outcome was achieved exclusively in the 4× HA condition and is consistent with the ability of HA to stimulate VEGF production in other cell types (34), but not previously found in the context of valvular disease. This increase in VEGF could play a role in stimulating the angiogenesis seen in valve disease; valves are normally avascular, but angiogenesis is thought to occur during CAVD to compensate for diffusion limitations introduced by leaflet thickening.

Based upon evidence that oxLDL deposition also appears as an early event in CAVD and that lipoproteins are preferentially retained in areas enriched in proteoglycans in heart valves (35) and atherosclerotic vessels (36), we next examined whether GAG enrichment indirectly stimulated pathological VIC behavior via differential regulation of lipoprotein deposition. We did indeed find that LDL and oxLDL depositions were enhanced in GAG-enriched environments. The ability to retain LDL or oxLDL was not equivalent across the two GAGs examined in our study, with significantly greater LDL and oxLDL deposition occurring in the CS-enriched platform. The oxLDL retained on CS-enriched substrates was able to overcome the antiinflammatory properties of the CS alone and induce an increase in the production of inflammatory cytokines by VICs. Therefore, it appears that CS enrichment contributes to disease progression by enabling oxLDL deposition that, in turn, drives inflammatory activity. Although retention of LDL was also increased by CS enrichment, it did not stimulate increased inflammatory activity or VIC activation.

Despite the focus on targeting cholesterol and lipid metabolism in the ongoing search for a CAVD treatment (27, 37, 38), relatively little is known about the effect of lipoproteins on VIC function. Our findings implicate oxLDL as a potent factor in regulating pathological VIC behavior: Even in the absence of

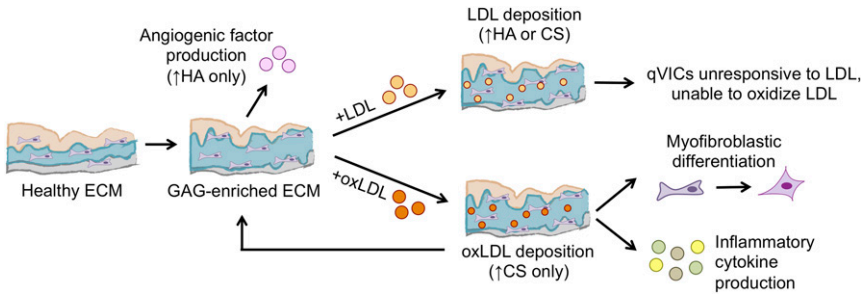

Fig. 8. Schematic of proposed sequence of events in early CAVD. Our findings indicate distinct and separate roles for individual GAGs in events related to disease progression. HA enrichment induces VIC secretion of VEGF, an angiogenic cytokine, while CS enrichment leads to increased deposition of oxidized lipoproteins, which, in turn, induce myofibroblastic activation and the production of inflammatory cytokines. Deposited oxLDL can also further stimulate GAG production, thereby forming a positive feedback loop for increased lipoprotein deposition and subsequent pathological events. Both HA and CS enrichment supported unoxidized LDL deposition, but quiescent VICs were generally unresponsive to LDL and unable to oxidize it themselves.

GAG enrichment, exposure to oxLDL in our study increased VIC production of multiple inflammatory cytokines known to be present in diseased valves (11). For example, IL-6 is highly expressed in calcified aortic valves and is believed to participate in the process of osteogenic VIC transformation (39). However, the present study demonstrates that these cytokines are both produced by VICs and present in the early-diseased valve environment, before the arrival of macrophages. Treatment with oxLDL in our study also induced a VIC phenotype consistent with myofibroblastic differentiation. Although others have not found increased myofibroblastic VIC differentiation upon oxLDL treatment (40), the previous study employed traditional VIC culture methods that produce a largely myofibroblastic population before oxLDL administration, which would likely diminish their ability to further elevate myofibroblastic markers in response to this stimulus. In contrast to previous work (40–43), we also did not find evidence of osteogenic VIC differentiation in response to oxLDL treatment. However, this again could be due to a difference in the starting phenotype of the VICs, as other studies that treated VICs with oxLDL used either traditionally cultured (i.e., myofibroblastic) VICs (40, 43) or VICs primed with osteogenic media (41, 42). These differences can complicate the ability to make cross-study comparisons, but they also raise the interesting possibility that VIC responsiveness to oxLDL is dependent upon VIC phenotype, which could have implications for understanding the role of oxLDL in disease progression. Regarding the source of oxLDL initially retained in early valve lesions, the inability of either quiescent VICs or valvular endothelial cells (VECs) to oxidize LDL (Fig. S3) leads us to postulate that it is derived from circulating oxLDL. Additional support for this hypothesis comes from observations that increased plasma levels of circulating oxLDL are associated with increased fibrocalcific remodeling in CAVD (44), and conditions with increased circulating oxLDL levels are known to be risk factors for CAVD (45–49). LDL that is retained in the early valve lesion may be oxidized later in the disease process by macrophages (50) or potentially by myofibroblastic VICs, although the latter possibility has not yet been examined. Overall, the crucial role for oxidized lipoproteins in dictating VIC fate and coordinating the progression of multiple features of early valve disease also supports the recent emergence of lipoprotein(a) [Lp(a)] as a novel drug target for the treatment of CAVD (51–53).

In contrast to the potent effects of oxLDL on VICs, treatment with LDL had little effect on VIC phenotype or inflammation. These results suggest that VICs exhibit a different response to LDL than vascular smooth muscle cells (SMCs), which is pertinent to understanding potential differences between lesion development in CAVD and atherosclerosis. Our proposed sequence of events in valvular pathology exhibits many commonalities with the widely studied "response to retention" model of atherosclerosis (54). However, differences in the abilities of VICs and SMCs to interact with unoxidized lipoproteins may represent a critical point of divergence of these two pathologies. Unlike the quiescent VICs which populate early valve lesions, SMCs respond to LDL via increased production of inflammatory factors (55, 56) and are able to oxidize LDL themselves (57). This dissimilarity could be relevant in understanding, for example, why statin drugs are effective at lowering the incidence of atherosclerosis (58, 59) (i.e., where SMCs are responsive to LDL) but not effective at inhibiting CAVD (60) (i.e., where VICs are not responsive to LDL and are unable to oxidize it themselves).

In addition to increasing both inflammatory activity and VIC activation, oxLDL increased GAG deposition, thereby creating a positive feedback loop in this sequence of events (Fig. 7) where GAG enrichment drives oxLDL deposition, which then drives further GAG enrichment. Others have also reported an increase in biglycan expression as a direct result of oxLDL treatment (43). The present work did not seek to evaluate causes of initial GAG dysregulation, but it is likely that CS enrichment initially precedes oxLDL deposition in the pathological cascade because healthy substrates did not support lipoprotein retention at sufficient levels to induce any of the disease features evaluated in this study. Although further work will be necessary to confirm the importance of the aforementioned positive feedback loop, it emerges as a potential therapeutic target to halt CAVD progression. Others have previously proposed GAG synthesis pathways as potential targets for the treatment of valve disease (61).

The findings in this study were enabled by the construction of a unique platform for studying the interactions of microenvironmental changes and physiological events that are relevant to early CAVD. Throughout this work, HA and CS exerted different effects on the measured outcomes: The most prominent result of HA enrichment was an increase in VEGF production, whereas CS was ultimately more potent in its ability to retain oxLDL. These findings suggest distinct and separate roles for each of these GAGs in the process of valve lesion development, with HA directly stimulating factors that may contribute to the angiogenesis seen in later disease stages and CS indirectly stimulating VIC differentiation and inflammatory pathways. The ability to dissect out the individual contributions of specific microenvironmental cues could have powerful consequences for elucidating the complex array of mechanisms and cellular decision-making processes that drive these pathological outcomes. This report also describes VIC culture in a CS-based environment, which is uncommon, despite methacrylation of CS and HA being equally practical (62, 63). Thus, this study points to the crucial role that CS plays in the progression of early CAVD and highlights the importance of expanding the examination of GAGs in the aortic valve beyond HA.

Of course, our approach is not without limitations. This work studied only a narrow window of events related to CAVD; it did not include investigation of factors regulating the onset of GAG enrichment or the importance of early-stage characteristics in progressing to later-stage events, such as fibrosis and/or calcification. Additionally, although they are arguably the most prominent features of early lesion development, the increases in HA and CS represent only two of the changes that occur during early CAVD. While the goal of the present work was to focus on how these ECM cues affect subsequent pathological events, changes in tissue mechanics may also make important contributions to the cellular behaviors examined herein. Scaffold mechanics can easily be adjusted using the GelMA/GAG materials, and future studies can expand the complexity of this approach through simultaneous variation of ECM cues and stiffness. With respect to mimicking other features of the early valve lesion, one of the primary limitations on this front is our incomplete knowledge of other early lesion characteristics. We examined our pig model of early leaflet thickening for evidence of TGF-β1 or TNFα, whose presence has been documented in later-stage CAVD (64), but we did not find an increase in gene expression (11) or deposition (Fig. S7) of these factors. Results from our in vitro studies were consistent with this observation, as TGF-β1 production was unaffected by either GAG enrichment or LDL/oxLDL treatment (Fig. S7). The absence of TGF-β1 elevation during early-stage events is potentially interesting on its own, as delivery of this molecule is perhaps the most common approach for studying VIC pathology in vitro (65), yet our results indicate that such an approach may not be appropriate for mimicking the early lesion environment.

There are also limitations associated with the sources of the biomaterials employed in this platform. This study was performed using HA of one specific molecular mass range (100 kDa) and the biological functions of HA are known to be dependent on molecular mass (16, 66). Thus, it is possible that different results would be observed if these studies were repeated with HA of a different molecular mass. Similarly, the VIC

response to CS could be affected by modifications in chain length or sulfation patterns. The CS in this study was purchased from a commercial source to ensure consistency and obtain the relatively large quantities needed for biomaterial fabrication. Of course, no in vitro system can perfectly mimic the native valve composition. However, despite these limitations, the biomaterial and culture environment described herein achieve increased complexity compared to previous work and allowed the elucidation of relationships that were previously unidentified in the context of VIC pathobiology.

Conclusions

We have generated a complex culture platform that mimics multiple characteristics found in early CAVD—namely, enriched GAGs, quiescent VICs, and presence of lipoproteins. Based upon our findings, we propose a sequence for several critical pathological events that have not previously been documented in VIC cultures (Fig. 8) and evidence for initiation of the inflammatory response by VICs in vivo. The connection of these events to the manifestation of clinical CAVD has yet to be determined; however, this approach to engineering a diseased environment yields a tailorable and controlled platform that may provide a basis for performing systematic studies of disease-related outcomes and can be extended to include additional CAVD risk factors and examine later-stage events in CAVD pathogenesis. These engineered environments may provide us with not only a means to decipher disease etiology, but also a platform for testing potential pharmacological treatments.

Materials and Methods

GelMA/GAG Hydrogel Synthesis. Gelatin methacrylation was performed as described by Loessner et al. (67). Gelatin from porcine skin (Sigma) was dissolved in PBS (10% wt/vol) at 55 °C followed by addition of methacrylic anhydride (Sigma) at a rate of 200 μL/min, using a peristaltic pump. The methacrylic anhydride was added to achieve a final concentration of 2.5%, 5%, or 10% wt/vol to yield GelMA with varied degrees of methacrylate functionalization. The methacrylation reaction was allowed to proceed overnight at 55 °C. After this incubation period, the solution was centrifuged at 3,500 × *g* for 5 min, and the supernatant containing GelMA was collected, diluted 1:4 in PBS, and transferred to 12- to 14-kDa MWCO dialysis tubing (Thermo Fisher Scientific). GelMA was then dialyzed against PBS for 3 d and deionized water for 2 d, sterile filtered, and lyophilized. CS (Sigma) was methacrylated following the same procedure, while HA (Fluka) was chemically modified with glycidyl methacrylate according to a protocol published by Leach et al. (68). All purified materials were stored at −20 °C.

GelMA/GAG substrates were fabricated via photopolymerization. Polymer solutions were prepared in sterile PBS and contained 0.05% photoinitiator lithium arylphosphonate (LAP) [synthesized as described elsewhere (69)], 5% (wt/vol) GelMA, and methacrylated HA or CS at either 2.4 mg/mL or 9.6 mg/mL. Although the GelMA concentration remained constant for all formulations, GelMA batches with different degrees of functionalization were mixed to maintain a constant Young's modulus. Dynamic mechanical analysis was performed using an MTS Insight 5 instrument. Disks 8 mm in diameter and 2 mm thick were tested at room temperature, and the elastic modulus was calculated from the stress–strain curve obtained at a frequency of 1 Hz. Thus, the mechanical properties of the substrates remained constant even when the GAG content increased.

For the remaining experiments, 15 μL of GelMA/GAG prepolymer solution was dispensed onto a parafilm stage, and a 15-mm glass coverslip (Electron Microscopy Sciences) was applied onto the drop in a sandwich configuration; this assembly was exposed to UV light at 365 nm for 5 min, using a Black-Ray XX-15L lamp (3 mW/cm^2, 115 V, 60 Hz; UVP). After cross-linking, the coverslips were carefully peeled off the parafilm, resulting in the formation of a thin (100–200 μm) hydrogel layer over the glass surface. Gels were allowed to swell overnight in PBS and UV sterilized at 254 nm for 1 h before use.

VIC Isolation, Culture, and Treatment. Aortic valve leaflets were excised from porcine hearts obtained from a local abattoir (Hoesly's) and VICs were isolated through collagenase digestion as described previously (70, 71). The isolated cells were plated and expanded on tissue culture polystyrene in low-glucose Dulbecco's modified Eagle's medium (DMEM) (Sigma) supplemented with 10% heat-inactivated FCS (Sigma), 150 units/mL penicillin/streptomycin (Sigma), and 2 mM L-glutamine (Sigma). Once the VICs were ∼90% confluent, they were passaged and cultured on collagen-I–coated TCPS [2 μg/cm^2; Advanced BioMatrix (72)] in low-glucose DMEM supplemented with 2% heat-inactivated FCS, 5.25 μg/mL insulin, 10 ng/mL FGF-2 (PeproTech), 150 units/mL penicillin/streptomycin, and 2 mM L-glutamine. These culture conditions produce VICs that exhibit a quiescent phenotype, which is consistent with the phenotype of VICs found in native valves (71). After 9 d in culture, VICs were seeded on either GelMA only or GelMA/GAG hydrogels in medium containing 2% FCS, 150 units/mL penicillin/streptomycin, and 2 mM L-glutamine. A subset of experiments was also repeated using naive VICs, which were seeded for experimentation immediately after isolation, without any prior culturing. Cells were plated at a density of 50,000 cells/cm^2 with the exception of the proliferation experiments, for which VICs were seeded at 20,000 cells/cm^2. To determine the effect of lipoprotein treatment on VIC phenotype and function, VICs seeded on GelMA hydrogels (without GAGs) were treated with 25 μg/mL human LDL (RayBiotech) or oxLDL (Athens Research & Technology). In all experiments, samples were collected for analysis 72 h after cell seeding.

Evaluation of Cell Phenotype. VIC proliferation was assessed using a Click-iT EdU Alexa Fluor 488 Imaging kit (Invitrogen). After incubation with EdU for 16 h, manufacturer's instructions were followed to label proliferating cells, and fluorescent images were captured using an Olympus IX51 microscope. Using ImageJ software for analysis, the percentage of proliferating cells was determined by dividing the number of proliferating cells by the total number of cells determined through DAPI counterstaining. Apoptosis was evaluated with the SensoLyte Homogeneous AFC Caspase 3/7 Assay kit (AnaSpec) following the manufacturer's instructions. Fluorescence was quantified using a Tecan Infinite M1000 plate reader and divided by the average number of cells in each condition, as determined by DAPI staining. The level of apoptosis in each condition was then normalized to the GelMA control for each experiment.

The extent of myofibroblastic VIC activation was evaluated through quantification of αSMA (αSMA/ACTA2) gene expression levels via qRT-PCR. VIC RNA was isolated with an RNEasy mini kit (Qiagen) and reverse transcribed with a High Capacity cDNA Reverse Transcription kit (Applied Biosystems). An *ACTA2* Taqman Gene Expression Assay (Applied Biosystems) was employed for qRT-PCR, using *GAPDH* as the endogenous control. Osteogenic differentiation of VICs was similarly evaluated, using Taqman kits for alkaline phosphatase (ALP) and bone morphogenetic protein-2 (BMP2). Data were analyzed using the relative standard curve C_T method and normalized to the GelMA control for each experiment.

Quantification of Inflammatory and Angiogenic Cytokine Production. The concentrations of various inflammatory and angiogenic cytokines in VIC culture supernatants were quantified through ELISAs. The production of PDGF-BB (Peprotech), IL-6 (R&D Systems), IL-8 (R&D Systems), monocyte chemoattractant protein (MCP-1; RayBiotech), VEGF (R&D Systems), and TGF-β1 (R&D Systems) was assessed according to the manufacturer's instructions and normalized to the average number of cells in each condition determined through DAPI staining.

Quantification of Lipoprotein Deposition. To quantify lipoprotein deposition on GelMA/GAG hydrogels, LDL and oxLDL were fluorescently labeled using an Alexa Fluor 488 Protein Labeling Kit (Thermo Scientific). GelMA and GelMA/GAG hydrogels were synthesized as described above and allowed to swell overnight in PBS. At that point, 25 μg/mL of fluorescently labeled LDL or oxLDL diluted in PBS was added to each film and incubated at 37 °C. After 48 h, the hydrogels were rinsed four times with PBS and fluorescence intensity was measured at six different spots per gel, using a Tecan Infinite M1000 plate reader. The average intensity for each substrate composition was calculated to obtain the relative levels of lipoprotein retention.

VIC Culture on Hydrogels Containing Deposited Lipoproteins. To study the effect of deposited lipoproteins on VICs, GelMA and GelMA/GAG hydrogels were allowed to swell overnight and incubated in PBS containing 200 μg/mL of unlabeled LDL or oxLDL for 24 h. To remove unbound lipoproteins, gels were rinsed four times with sterile PBS and VICs were seeded as described above. Inflammatory cytokine production and *ACTA2* gene expression were assessed 48 h after seeding and normalized to the no treatment control for the corresponding GelMA/GAG formulation.

Quantification of GAG Production Following Lipoprotein Treatment. The production of GAGs by VICs cultured on GelMA hydrogels and treated with 25 μg/mL LDL or oxLDL was assessed. The gene expression levels of CHSY1 and HAS3 were evaluated using Taqman primers for *CHSY1* and *HAS3* (Applied Biosystems) via qRT-PCR. The concentrations of sulfated GAGs (sGAGs) and HA

secreted into the media were also measured. Cell culture supernatants were lyophilized and resuspended in PBS to concentrate the samples, and the concentration of sGAGs was quantified via an alcian blue assay (73). The HA concentration in culture supernatants was analyzed through an HA test kit (Corgenix) following the manufacturer's instructions. Both sGAG and HA concentrations were normalized to the average number of cells in each condition determined through DAPI staining.

Detection of Inflammatory Cytokines in Diseased Leaflets. IL-6 and PDGF-BB were detected via immunohistochemical staining of formalin-fixed, paraffin-embedded leaflet sections from 1yo WT swine or 1yo swine with familial hypercholesterolemia (1yo RFH). Tissue sections were deparaffinized and antigen retrieval was performed in citric acid buffer (pH 6.0; Vector Laboratories) for 2 h in a water bath at 80 °C. Blocking and detection of IL-6 (10 μg/mL, mouse IgG, Clone 77830; R&D Systems) and PDGF-BB (5 μg/mL, goat polyclonal; LifeSpan Biosciences) were performed using immunohistochemical methods, following the VECTASTAIN Elite ABC Kit protocol for mouse and goat, respectively (Vector Laboratories). Macrophages were detected with an anti-pig macrophages antibody (10 μg/mL, mouse IgG, Clone BA4D5; Bio-Rad) and fluorescent labeling using the VectaFluor DyLight 488 anti-mouse kit (Vector Labs). Bright-field and fluorescent images were captured using an Olympus IX51 microscope (Olympus). Levels of chromagen indicating positive staining were analyzed semiquantitatively using ImageJ software (NIH) following the protocol outlined by Balaoing et al. (74). The number of pixels that represent staining for an antigen was divided by the total sample area in pixels to generate the percentage of the tissue in the field of view that stained positively for a particular protein.

Statistics. Every experiment was conducted with $n = 3$–4 biological replicates, with VICs isolated from a total of 15 porcine hearts. Data are presented as mean ± SD. Experimental groups were compared using GraphPad Prism software with one-way ANOVA in conjunction with Tukey's honestly significant difference posttest. P values less than or equal to 0.05 were considered statistically significant.

ACKNOWLEDGMENTS. The authors acknowledge funding from the National Institutes of Health (R01 HL093281, R21 EB019508) and the American Heart Association (15PRE 22170006).

1. Go AS, et al.; American Heart Association Statistics Committee and Stroke Statistics Subcommittee (2013) Executive summary: Heart disease and stroke statistics–2013 update: A report from the American Heart Association. *Circulation* 127:143–152.
2. Li C, Xu S, Gotlieb AI (2013) The progression of calcific aortic valve disease through injury, cell dysfunction, and disruptive biologic and physical force feedback loops. *Cardiovasc Pathol* 22:1–8.
3. Rajamannan NM, et al. (2011) Calcific aortic valve disease: Not simply a degenerative process: A review and agenda for research from the National Heart and Lung and Blood Institute aortic stenosis working group. Executive summary: Calcific aortic valve disease-2011 update. *Circulation* 124:1783–1791.
4. Akat K, Borggrefe M, Kaden JJ (2009) Aortic valve calcification: Basic science to clinical practice. *Heart* 95:616–623.
5. Otto CM, Lind BK, Kitzman DW, Gersh BJ, Siscovick DS (1999) Association of aortic-valve sclerosis with cardiovascular mortality and morbidity in the elderly. *N Engl J Med* 341:142–147.
6. Völzke H, et al. (2010) Heart valve sclerosis predicts all-cause and cardiovascular mortality. *Atherosclerosis* 209:606–610.
7. Rajamannan NM, et al. (2010) Executive summary from the NHLBI working group on calcific aortic stenosis. *Circulation* 124:1783–1791.
8. Freeman RV, Otto CM (2005) Spectrum of calcific aortic valve disease: Pathogenesis, disease progression, and treatment strategies. *Circulation* 111:3316–3326.
9. Chen JH, Simmons CA (2011) Cell-matrix interactions in the pathobiology of calcific aortic valve disease: Critical roles for matricellular, matricrine, and matrix mechanics cues. *Circ Res* 108:1510–1524.
10. Hinton RB, Jr, et al. (2006) Extracellular matrix remodeling and organization in developing and diseased aortic valves. *Circ Res* 98:1431–1438.
11. Porras AM, et al. (2015) Development of aortic valve disease in familial hypercholesterolemic swine: Implications for elucidating disease etiology. *J Am Heart Assoc* 4: e002254.
12. Otto CM, Kuusisto J, Reichenbach DD, Gown AM, O'Brien KD (1994) Characterization of the early lesion of 'degenerative' valvular aortic stenosis. Histological and immunohistochemical studies. *Circulation* 90:844–853.
13. Sider KL, et al. (2014) Evaluation of a porcine model of early aortic valve sclerosis. *Cardiovasc Pathol* 23:289–297.
14. O'Brien KD, et al. (1996) Apolipoproteins B, (a), and E accumulate in the morphologically early lesion of 'degenerative' valvular aortic stenosis. *Arterioscler Thromb Vasc Biol* 16:523–532.
15. Stephens EH, et al. (2011) Differential proteoglycan and hyaluronan distribution in calcified aortic valves. *Cardiovasc Pathol* 20:334–342.
16. Rodriguez KJ, Piechura LM, Masters KS (2011) Regulation of valvular interstitial cell phenotype and function by hyaluronic acid in 2-D and 3-D culture environments. *Matrix Biol* 30:70–82.
17. Masters KS, Shah DN, Leinwand LA, Anseth KS (2005) Crosslinked hyaluronan scaffolds as a biologically active carrier for valvular interstitial cells. *Biomaterials* 26: 2517–2525.
18. Puperi DS, et al. (2016) Hyaluronan hydrogels for a biomimetic spongiosa layer of tissue engineered heart valve scaffolds. *Biomacromolecules* 17:1766–1775.
19. Rodriguez KJ, Piechura LM, Porras AM, Masters KS (2014) Manipulation of valve composition to elucidate the role of collagen in aortic valve calcification. *BMC Cardiovasc Disord* 14:29.
20. Liu AC, Gotlieb AI (2008) Transforming growth factor-beta regulates in vitro heart valve repair by activated valve interstitial cells. *Am J Pathol* 173:1275–1285.
21. Liu AC, Joag VR, Gotlieb AI (2007) The emerging role of valve interstitial cell phenotypes in regulating heart valve pathobiology. *Am J Pathol* 171:1407–1418.
22. Latif N, Sarathchandra P, Chester AH, Yacoub MH (2015) Expression of smooth muscle cell markers and co-activators in calcified aortic valves. *Eur Heart J* 36:1335–1345.
23. Porras AM, et al. (2017) Robust generation of quiescent porcine valvular interstitial cell cultures. *J Am Heart Assoc* 6:e005041.
24. Lindman BR, et al. (2016) Calcific aortic stenosis. *Nat Rev Dis Primers* 2:16006.
25. Coté N, et al. (2013) Inflammation is associated with the remodeling of calcific aortic valve disease. *Inflammation* 36:573–581.
26. Mohty D, et al. (2008) Association between plasma LDL particle size, valvular accumulation of oxidized LDL, and inflammation in patients with aortic stenosis. *Arterioscler Thromb Vasc Biol* 28:187–193.
27. Parisi V, et al. (2015) The lipid theory in the pathogenesis of calcific aortic stenosis. *Nutr Metab Cardiovasc Dis* 25:519–525.
28. Vallières M, du Souich P (2010) Modulation of inflammation by chondroitin sulfate. *Osteoarthritis Cartilage* 18:S1–S6.
29. Cuff CA, et al. (2001) The adhesion receptor CD44 promotes atherosclerosis by mediating inflammatory cell recruitment and vascular cell activation. *J Clin Invest* 108: 1031–1040.
30. Sadowitz B, Seymour K, Gahtan V, Maier KG (2012) The role of hyaluronic acid in atherosclerosis and intimal hyperplasia. *J Surg Res* 173:e63–e72.
31. Jain M, et al. (1996) Role of CD44 in the reaction of vascular smooth muscle cells to arterial wall injury. *J Clin Invest* 98:877.
32. Hjortnaes J, et al. (2016) Simulation of early calcific aortic valve disease in a 3D platform: A role for myofibroblast differentiation. *J Mol Cell Cardiol* 94:13–20.
33. Duan B, Yin Z, Hockaday Kang L, Magin RL, Butcher JT (2016) Active tissue stiffness modulation controls valve interstitial cell phenotype and osteogenic potential in 3D culture. *Acta Biomater* 36:42–54.
34. Murphy JF, et al. (2005) Engagement of CD44 modulates cyclooxygenase induction, VEGF generation, and proliferation in human vascular endothelial cells. *FASEB J* 19: 446–448.
35. Neufeld EB, et al. (2014) Decorin and biglycan retain LDL in disease-prone valvular and aortic subendothelial intimal matrix. *Atherosclerosis* 233:113–121.
36. Viola M, et al. (2016) Extracellular matrix in atherosclerosis: Hyaluronan and proteoglycans insights. *Curr Med Chem* 23:2958–2971.
37. Chan KL, Teo K, Dumesnil JG, Ni A, Tam J; ASTRONOMER Investigators (2010) Effect of lipid lowering with rosuvastatin on progression of aortic stenosis: Results of the aortic stenosis progression observation: Measuring effects of rosuvastatin (ASTRONOMER) trial. *Circulation* 121:306–314.
38. Rajamannan NM, Greve AM, Moura LM, Best P, Wachtell K (2015) SALTIRE-RAAVE: Targeting calcific aortic valve disease LDL-density-radius theory. *Expert Rev Cardiovasc Ther* 13:355–367.
39. El Husseini D, et al. (2014) P2Y2 receptor represses IL-6 expression by valve interstitial cells through Akt: Implication for calcific aortic valve disease. *J Mol Cell Cardiol* 72: 146–156.
40. Zeng Q, et al. (2014) Augmented osteogenic responses in human aortic valve cells exposed to oxLDL and TLR4 agonist: A mechanistic role of Notch1 and NF-κB interaction. *PLoS One* 9:e95400.
41. Nsaibia MJ, et al. (2017) OxLDL-derived lysophosphatidic acid promotes the progression of aortic valve stenosis through a LPAR1-RhoA-NF-kappaB pathway. *Cardiovasc Res* 113:1351–1363.
42. Li F, Zhao Z, Cai Z, Dong N, Liu Y (2015) Oxidized low-density lipoprotein promotes osteoblastic differentiation of valvular interstitial cells through RAGE/MAPK. *Cardiology* 130:55–61.
43. Song R, et al. (2012) Biglycan induces the expression of osteogenic factors in human aortic valve interstitial cells via toll-like receptor-2. *Arterioscler Thromb Vasc Biol* 32: 2711–2720.
44. Côté C, et al. (2008) Association between circulating oxidised low-density lipoprotein and fibrocalcific remodelling of the aortic valve in aortic stenosis. *Heart* 94:1175–1180.
45. Holvoet P, Lee DH, Steffes M, Gross M, Jacobs DR, Jr (2008) Association between circulating oxidized low-density lipoprotein and incidence of the metabolic syndrome. *JAMA* 299:2287–2293.
46. Pandya V, Rao A, Chaudhary K (2015) Lipid abnormalities in kidney disease and management strategies. *World J Nephrol* 4:83–91.
47. Katz R, et al. (2006) Features of the metabolic syndrome and diabetes mellitus as predictors of aortic valve calcification in the Multi-Ethnic Study of Atherosclerosis. *Circulation* 113:2113–2119.
48. Towler DA (2013) Molecular and cellular aspects of calcific aortic valve disease. *Circ Res* 113:198–208.

49. Kamath AR, Pai RG (2008) Risk factors for progression of calcific aortic stenosis and potential therapeutic targets. *Int J Angiol* 17:63–70.
50. Parthasarathy S, Raghavamenon A, Garelnabi MO, Santanam N (2010) Oxidized low-density lipoprotein. *Methods Mol Biol* 610:403–417.
51. Capoulade R, et al. (2015) Oxidized phospholipids, lipoprotein(a), and progression of calcific aortic valve stenosis. *J Am Coll Cardiol* 66:1236–1246.
52. Rogers MA, Aikawa E (2015) A not-so-little role for lipoprotein(a) in the development of calcific aortic valve disease. *Circulation* 132:621–623.
53. Thanassoulis G (2016) Lipoprotein (a) in calcific aortic valve disease: From genomics to novel drug target for aortic stenosis. *J Lipid Res* 57:917–924.
54. Tabas I, Williams KJ, Borén J (2007) Subendothelial lipoprotein retention as the initiating process in atherosclerosis: Update and therapeutic implications. *Circulation* 116:1832–1844.
55. Ryoo SW, et al. (2004) Native LDL induces interleukin-8 expression via H2O2, p38 kinase, and activator protein-1 in human aortic smooth muscle cells. *Cardiovasc Res* 62:185–193.
56. Stiko-Rahm A, Hultgårdh-Nilsson A, Regnström J, Hamsten A, Nilsson J (1992) Native and oxidized LDL enhances production of PDGF AA and the surface expression of PDGF receptors in cultured human smooth muscle cells. *Arterioscler Thromb* 12: 1099–1109.
57. Morel DW, DiCorleto PE, Chisolm GM (1984) Endothelial and smooth muscle cells alter low density lipoprotein in vitro by free radical oxidation. *Arteriosclerosis* 4:357–364.
58. SSSS Group (1994) Randomised trial of cholesterol lowering in 4444 patients with coronary heart disease: The Scandinavian Simvastatin Survival Study (4S). *Lancet* 344: 1383–1389.
59. Baigent C, et al.; Cholesterol Treatment Trialists' (CTT) Collaboration (2010) Efficacy and safety of more intensive lowering of LDL cholesterol: A meta-analysis of data from 170,000 participants in 26 randomised trials. *Lancet* 376:1670–1681.
60. Zhao Y, Nicoll R, He YH, Henein MY (2016) The effect of statins on valve function and calcification in aortic stenosis: A meta-analysis. *Atherosclerosis* 246:318–324.
61. Grande-Allen KJ, et al. (2007) Glycosaminoglycan synthesis and structure as targets for the prevention of calcific aortic valve disease. *Cardiovasc Res* 76:19–28.
62. Abbadessa A, et al. (2016) A thermo-responsive and photo-polymerizable chondroitin sulfate-based hydrogel for 3D printing applications. *Carbohydr Polym* 149:163–174.
63. Hayami JW, Waldman SD, Amsden BG (2016) Chondrocyte generation of cartilage-like tissue following photoencapsulation in methacrylated polysaccharide solution blends. *Macromol Biosci* 16:1083–1095.
64. Jian B, Narula N, Li QY, Mohler ER, 3rd, Levy RJ (2003) Progression of aortic valve stenosis: TGF-beta1 is present in calcified aortic valve cusps and promotes aortic valve interstitial cell calcification via apoptosis. *Ann Thorac Surg* 75:457–465; discussion 465–466.
65. Miller JD, Weiss RM, Heistad DD (2011) Calcific aortic valve stenosis: Methods, models, and mechanisms. *Circ Res* 108:1392–1412.
66. Singleton PA (2014) Hyaluronan regulation of endothelial barrier function in cancer. *Adv Cancer Res* 123:191–209.
67. Loessner D, et al. (2016) Functionalization, preparation and use of cell-laden gelatin methacryloyl-based hydrogels as modular tissue culture platforms. *Nat Protoc* 11: 727–746.
68. Leach JB, Bivens KA, Collins CN, Schmidt CE (2004) Development of photocrosslinkable hyaluronic acid-polyethylene glycol-peptide composite hydrogels for soft tissue engineering. *J Biomed Mater Res A* 70:74–82.
69. Fairbanks BD, Schwartz MP, Bowman CN, Anseth KS (2009) Photoinitiated polymerization of PEG-diacrylate with lithium phenyl-2,4,6-trimethylbenzoylphosphinate: Polymerization rate and cytocompatibility. *Biomaterials* 30:6702–6707.
70. Johnson CM, Hanson MN, Helgeson SC (1987) Porcine cardiac valvular subendothelial cells in culture: Cell isolation and growth characteristics. *J Mol Cell Cardiol* 19: 1185–1193.
71. Latif N, et al. (2015) Modulation of human valve interstitial cell phenotype and function using a fibroblast growth factor 2 formulation. *PLoS One* 10:e0127844.
72. Rodriguez KJ, Masters KS (2009) Regulation of valvular interstitial cell calcification by components of the extracellular matrix. *J Biomed Mater Res A* 90:1043–1053.
73. Frazier SB, Roodhouse KA, Hourcade DE, Zhang L (2008) The quantification of glycosaminoglycans: A comparison of HPLC, carbazole, and alcian blue methods. *Open Glycosci* 1:31–39.
74. Balaoing LR, Post AD, Liu H, Minn KT, Grande-Allen KJ (2014) Age-related changes in aortic valve hemostatic protein regulation. *Arterioscler Thromb Vasc Biol* 34:72–80.